



ELSEVIER

Available online at [www.sciencedirect.com](http://www.sciencedirect.com)

SCIENCE @ DIRECT®

Journal of  
Electroanalytical  
Chemistry

Journal of Electroanalytical Chemistry 554–555 (2003) 99–111

[www.elsevier.com/locate/jelechem](http://www.elsevier.com/locate/jelechem)

# Electrochemical and surface characterization of platinum silicide electrodes and their use as stable platforms for electrogenerated chemiluminescence assays

Eve F. Fabrizio, Todd M. McEvoy, Priya Jassel, Jose Lozano, Keith J. Stevenson, Allen J. Bard\*

*Department of Chemistry and Biochemistry, University of Texas at Austin, Austin, TX 78712, USA*

Received 21 October 2002; received in revised form 10 January 2003; accepted 20 January 2003

## Abstract

Electrochemical methods, including cyclic voltammetry and scanning electrochemical microscopy, as well as surface techniques, including conductive atomic force microscopy (AFM) and X-ray photoelectron spectroscopy, were utilized to evaluate and characterize the extent of an oxide layer on platinum silicide (PtSi) surfaces that were pretreated by a variety of approaches; piranha solution (1:4 H<sub>2</sub>O<sub>2</sub>+H<sub>2</sub>SO<sub>4</sub>), hydrofluoric acid (HF), chemical reduction in NaBH<sub>4</sub> and after mechanically polishing the surface. Electrochemical methods showed that in the presence of an oxide layer, the rate of electron transfer depended upon the charge of the redox couple: the more negative the charge, the slower is the rate of electron transfer. Additionally, the current levels observed in the presence of an extensive oxide layer were considerably lower than those observed after the oxide layer was removed either with HF acid or by mechanically polishing. Surface analysis and depth profiles obtained using Auger electron spectroscopy demonstrated that PtSi surfaces pretreated with piranha contained the largest amounts of surface oxides. AFM topographic scans along with localized surface conductivity showed that in the presence of this oxide layer, electron transfer occurred at nanoscale domains located between the PtSi grains with the rest of the surface, which most likely contains an oxide layer, being non-conductive. The surface oxide layer was used to attach the electrogenerated chemiluminescent (ECL) label, Ru(bpy)<sub>3</sub><sup>2+</sup> covalently, either directly or via single-stranded DNA. Emission during oxidation in the presence of the co-reactant tri-*n*-propylamine was observed, illustrating the possible use of PtSi as a platform for ECL-based bioassays.

© 2003 Elsevier Science B.V. All rights reserved.

**Keywords:** Platinum silicide; Disk electrodes; Charge transfer kinetics; Electroluminescence

## 1. Introduction

Silicides are of great interest as low-cost stable materials for solid-state microelectronics and as radiation detectors [1–6]. In particular, by incorporating noble metals such as platinum into silicon, the polysilicon interconnect resistance can be reduced, therefore, providing low-resistance ohmic contacts for transistors. As device dimensions reach the sub-micron range, one must determine whether electrical and mechanical integrity of the silicide is maintained. As a result,

numerous studies have characterized the kinetics of phase formation, final composition, microstructure and electron structure of sub-half micron thin platinum silicide (PtSi) films. Additionally, PtSi has been studied as an alternative electrode for hydrogen evolution and water electrolysis [7–9]. Even though previous studies by these groups have centered on obtaining enhanced rates of electrolysis, they also evaluated structural stability with extreme potential biasing. PtSi has also been used to protect Si electrodes in photoelectrochemical cells, even allowing the photogeneration of chlorine [10,11]. Overall, PtSi has been shown to possess electrical and chemical properties that are similar to those of pure platinum: low resistivity and nominal corrosion during electrolysis. It is these physical properties, along with the

\* Corresponding author. Tel.: +1-512-471-3761; fax: +1-512-471-0088.

E-mail address: [ajbard@mail.utexas.edu](mailto:ajbard@mail.utexas.edu) (A.J. Bard).

possibility of having a surface oxide layer, which make PtSi a workable material for use as array electrodes in electrophoretic microdevices and electrochemical biosensors.

While a small number of studies has evaluated the current vs. voltage curves of PtSi in aqueous electrolytes, none of these studies has closely evaluated the electrochemical properties of this alloy, specifically, the heterogeneous electron transfer observed at the surface of these films [12–14]. Previous surface analysis and depth profiling obtained using a variety of X-ray photoelectron spectroscopy (XPS) methods have determined that PtSi annealed in a conventional furnace contains a three-layer structure, a top monolayer of atomic Pt and SiO<sub>2</sub>, an underlying monolayer of Pt<sub>x</sub>Si<sub>y</sub> (where  $x > y$ ), and a bulk layer of PtSi [15–26]. All three layers vary in structure and thickness based on the annealing conditions; atmosphere, temperature, and time [15]. The goal of this work was to investigate the electrochemical properties of PtSi after a number of standard pretreatments to determine the viability of PtSi films for future use in electrochemical microdevices and sensors. In particular, we were interested in using surface-sensitive electrochemical methods, such as cyclic voltammetry (CV) and scanning electrochemical microscopy (SECM), in addition to surface techniques, such as Auger electron spectroscopy (AES) and conductive atomic force microscopy (AFM), to characterize the chemical and electrochemical surface properties of these films.

## 2. Experimental

### 2.1. Chemicals and materials

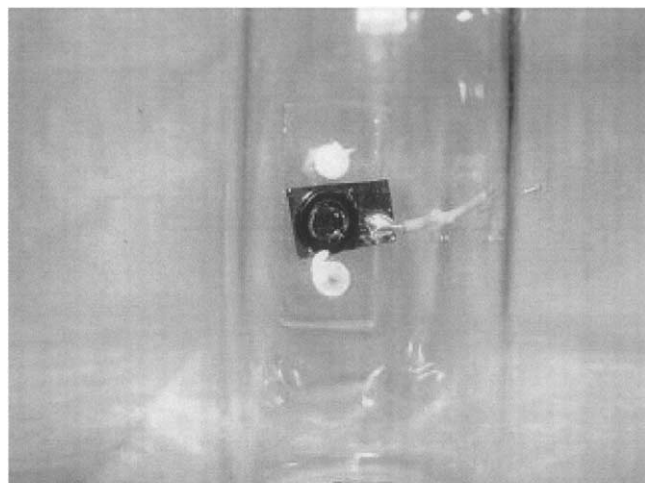
Platinum silicide (PtSi) wafers were obtained from Nanogen, Inc. (San Diego, CA). The wafers were prepared by sputtering 500 Å of Si and 500 Å of Pt at 1000 W under an inert atmosphere onto a plasma-cleaned oxidized silicon wafer using a Perkin–Elmer 4480 Production Sputtering System (Perkin–Elmer, Ultek Division, Palo Alto, CA). The platinum layer was then annealed into the silicon layer by heating the wafers at 420 °C for 30 min in an oxygen-free environment. Piranha solution was prepared by mixing one part hydrogen peroxide (Mallinckrodt, Paris, KY) to four parts concentrated sulfuric acid (Mallinckrodt, Phillipsburgh, NJ). (Caution: piranha solution is a very strong oxidizing agent and very dangerous to handle in the laboratory. Protective equipment including gloves, goggles, and face shields should be used at all times.) Hydrofluoric (HF) acid solutions (1%) used for etching SiO<sub>2</sub> were prepared by adding 10 µl of concentrated HF (48%; EM Sciences, Gibbstown, NJ) to 1 ml of Milli-Q water (Millipore Corp., Bedford, MA) (extreme care

should be taken when working with HF solutions). Small volumes (<1 ml) were prepared to minimize potential exposure and waste disposal. Sodium tetrahydroborate (or sodium borohydride (NaBH<sub>4</sub>); Aldrich, Milwaukee, WI) solutions at a concentration of 1 M were prepared by dissolving the appropriate weight into a given volume of Milli-Q water.

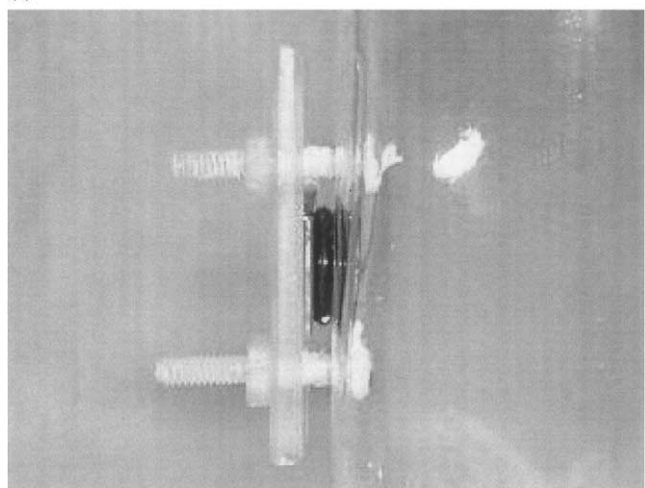
### 2.2. Electrochemical analysis on PtSi surfaces

PtSi wafers were diced or cut into 1 cm × 1 cm size chips with a diamond scribe. After the PtSi chips were first treated with piranha solution, electrical contact was made to one corner of the PtSi side of the chip using insulated nichrome-coated copper wire and silver epoxy (H2OE from EPO-TEK, Billerica, MA). The contact point was covered with 5 Minute Epoxy (ITW Devon Corp., Danvers, MA) to ensure that the silver epoxy was never in contact with the electrolyte during measurements. To verify good electrical contact, the resistance between the PtSi surface and the wire was tested with an ohmmeter. Some of the PtSi surfaces were then additionally treated by either etching off the SiO layer using 1% HF, reducing the surface with NaBH<sub>4</sub> or by mechanically polishing with 0.05 µm alumina and a microcloth (Buehler, Lake Bluff, IL). For the HF and NaBH<sub>4</sub> solutions, a small drop was placed onto the center of the surface of the PtSi surface and left there for a given amount of time: 30 s for 1% HF and 1 min for 1 M NaBH<sub>4</sub>. All chips were thoroughly rinsed with Milli-Q water and dried using a high-pressure nitrogen line prior to any experimental measurement.

To facilitate electrochemical measurement, all PtSi chips were mounted onto a special glass cell holder that contained a 3 mm diameter hole (area equal to 0.071 cm<sup>2</sup>). A front and side image of the cell is provided in Fig. 1. Each chip was placed in contact with the electrolyte solution by positioning it over the hole and by clamping it into place with a Plexiglas plate that was held in place by two Teflon screws. A Neoprene o-ring was positioned between the glass cell and the PtSi surface to eliminate electrolyte leakage. The rest of the electrochemical cell consisted of a platinum mesh counterelectrode and silver | silver chloride reference electrode (Ag | AgCl | KCl (sat.)). Prior to obtaining voltammograms, the PtSi surface was cycled approximately 40 times in 0.2 M H<sub>2</sub>SO<sub>4</sub> between 0.9 and –0.3 V versus Ag | AgCl | KCl (sat.). Voltammetric scans involving the hydrogen evolution reaction (her) were performed in 1.0 M H<sub>2</sub>SO<sub>4</sub> while the underpotential deposition (upd) of copper was performed in 0.2 M H<sub>2</sub>SO<sub>4</sub>. All additional voltammetry using a polycrystalline platinum surface was performed with a 1.5-mm diameter Pt disk electrode (BioAnalytical Systems, Indianapolis, IN) that was mechanically polished with



(a)



(b)

Fig. 1. Front (a) and side (b) images of the electrochemical cell used to obtain voltammetry and ECL at the PtSi surfaces.

0.05  $\mu\text{m}$  alumina and a microcloth (Buehler, Lake Bluff, IL).

### 2.3. SECM instrumentation and procedure

The basic experimental set-up used for the SECM measurements consisted of a CH Instruments 900 SECM (CH Instruments, Austin, TX). After the PtSi substrates were cleaned and pretreated using the same procedures discussed in the above section, they were mounted into a homemade Teflon SECM cell that exposed a circular area approximately 2 mm diameter (area = 0.031  $\text{cm}^2$ ) to facilitate tip access. The probe tip consisted of a 25- $\mu\text{m}$  diameter Pt disk ultramicroelectrode embedded in glass with a total radius of 40  $\mu\text{m}$ . This corresponds to an RG value (RG = total radius/radius of Pt disk) of  $\sim 3.5$ . The reference electrode was an Ag | AgCl | KCl (sat.) electrode and the counter-electrode was a Pt wire. Prior to the SECM measurements, the PtSi surface was cycled approximately 40

times in 0.2 M  $\text{H}_2\text{SO}_4$  between 0.9 and  $-0.3$  V versus Ag | AgCl | KCl (sat.) to be consistent with our voltammetric measurements. Using the SECM bipotentiostat, the electrochemical behavior of both the tip and substrates was evaluated by obtaining voltammograms of the solution redox couple prior to acquiring series of approach curves. Each approach curve was obtained by setting the tip to a potential at which a steady-state response is observed while the potential applied to the PtSi substrate was varied from approximately 1000 to 0 mV past the  $E^\circ$  depending on the redox couple being measured. The tip, which was driven by an inchworm, approached the substrate at a rate of 3  $\mu\text{m s}^{-1}$ . During each approach, the tip current as a function of distance was recorded. All electrochemical solutions were used without degassing and all measurements were obtained at room temperature.

### 2.4. Conductive probe AFM

Conductive probe AFM was carried out using a Digital Instruments Dimension 3100 in combination with a Nanoscope IV Controller (Veeco Metrology, Santa Barbara, CA). All measurements were obtained in contact mode using Pt/Ir-coated Si SPM probes (cantilever length—450  $\mu\text{m}$  and force constant—0.2  $\text{N m}^{-1}$ , model SCM-PIC, Veeco Metrology). Electrical contact to the sample was made with conductive Ag epoxy applied between the sample and the conductive chuck of the AFM stage. The scan head was fitted with a current sensing application module (TUNA-Tunneling AFM) manufactured by Digital Instruments to perform electrical characterization. The current sensitivity of the preamp employed was 10  $\text{pA V}^{-1}$ . Topography and conductivity images were acquired simultaneously while scanning at 0.5 Hz with an applied dc sample bias of +12 V. For better image clarity, a first-order flatten function was performed on the topographic image. Surface roughness of the topography image was estimated after applying a zero-order flattened function to the image to remove the influence of sample drift.

### 2.5. XPS analysis of PtSi surfaces

Prior to surface analysis, the PtSi wafer sample was pretreated by soaking the substrate in a piranha solution for 15 min, rinsing with de-ionized water and then drying with high-pressure nitrogen gas. An average depth profile was obtained using a PHI 5700 X-ray photoelectron spectrometer (Phymetrics, Eden Prairie, MN) with an Al monochromatic X-ray source at 1486.6 eV and a spectrometer pass energy set at 11.75 eV. The surface was sputtered using a PHI 04-303A Ar ion gun (Phymetrics, Eden Prairie, MN) with a beam energy of 3 kV and a sample current of 1  $\mu\text{A}$ . The UHV chamber had a base pressure of  $1 \times 10^{-10}$  Torr. To determine the

thickness of the sample, a  $2 \times 2$  mm spot was sputtered until the underlying  $\text{SiO}_2$  substrate was reached. With a sputtering rate of  $0.03 \text{ \AA s}^{-1}$ , the thickness of the PtSi layer was determined to be  $\sim 300 \text{ \AA}$ . A depth profile was then obtained by taking XPS data at  $20 \text{ \AA}$  intervals on a new spot. The raster size was also  $2 \times 2$  mm. Atomic concentrations on the PtSi surfaces were measured with the same X-ray source and resolution. The following energy ranges were analyzed: Pt 4f, 68–88 eV; Si 2p, 145–165 eV; O 1s, 525–545 eV. Scans were taken 0.1 eV per step and the time for each step was 1 s.

### 2.6. Electrogenerated chemiluminescence at oxidized PtSi surfaces

All electrogenerated chemiluminescence (ECL) measurements were obtained with a home-built system [27,28]. The system consisted of a photomultiplier tube (PMT, Hamamatsu R928) connected to a home-built current to voltage amplifier that was also used to measure the current being generated at the PtSi substrate during voltammetric scans. The potential of the substrate was controlled using an EG&G PAR 175 waveform generator. A data acquisition board and program from Labview (National Instruments, Austin, TX) was used to acquire the PMT current, electrode current, and potential during each scan. The same electrochemical cell as shown in Fig. 1 was used to acquire ECL. To facilitate the measurement of light, the PMT was positioned up against the glass cell and directly opposite the solution opening for the PtSi substrate.

To evaluate ECL from surface-attached  $\text{Ru}(\text{bpy})_3^{2+}$ , the PtSi surface was first silanized with either (3-aminopropyl)-trimethoxysilane or (4-aminobutyl)-dimethylmethoxysilane (Fluka, Milwaukee, WI). The silanization solution was prepared by mixing 500  $\mu\text{l}$  of the above silanizing agents with 500  $\mu\text{l}$  of Milli-Q water and 9.5 ml of ethanol (200 proof, Aaper Alcohol and Chem. Co., Shelbyville, KY). After the solution was mixed for 10 min, a drop of the silane solution was placed directly onto the PtSi surface and left in contact with the surface for 20 min. The surface was then rinsed with ethanol and dried with high-pressure nitrogen. The silanized PtSi surface was then placed in a  $100^\circ\text{C}$  oven for 30 min to complete the dehydration reaction.

The ECL label,  $\text{Ru}(\text{bpy}-\text{Me}_2)_2(\text{bpy}-(\text{COOH})_2)(\text{PF}_6)_2$ , was prepared by following a procedure provided in the literature [29]. The final compound was characterized using UV-vis spectroscopy, electrochemistry and elemental analysis. The UV-vis spectrum was similar to  $\text{Ru}(\text{bpy})_3\text{Cl}_2$  with a  $\lambda_{\text{max}}$  of 461 nm confirming the presence of three bipyridine ligands on the ruthenium. Voltammetry, however, exhibited two reversible oxidation waves at 1.1 and 1.4 V versus  $\text{Ag}|\text{AgCl}|\text{KCl}$  (sat.). The peak current of the first wave was twice that

of the second wave suggesting two products. The first wave at less positive potentials agrees with the oxidation of ruthenium with ligands containing methyl groups while the second wave at higher potential agrees with the oxidation of ruthenium with the ligands containing carboxylates [29–32]. Analysis calculated for  $\text{RuC}_{36}\text{H}_{32}\text{N}_6\text{O}_4\text{P}_2\text{F}_{12}$ : C, 43.1; H, 3.2; N, 8.4. Found: C, 43.4; H, 4.2; N, 8.7%. TLC performed with a number of solvents ( $\text{H}_2\text{O}$ , acetonitrile, and ethanol) showed only one product. Since only the ligands containing carboxylate groups can undergo further chemistry with surface amines, no further purification was attempted.

The carboxylate groups of the ruthenium complex were covalently attached to the aminosilane on the PtSi surface using the 1-ethyl-3-(3-dimethylaminopropyl)carbodiimide (EDC; Pierce, Rockford, IL). After mixing 10 mg of EDC into 10 ml of Milli-Q water and 2 mg of  $\text{Ru}(\text{bpy}-\text{Me}_2)_2(\text{bpy}-(\text{COOH})_2)^{2+}$  into 1 ml of 0.1 M MES (2-[*N*-morpholino]ethane sulfonic acid), pH 4.5, 500  $\mu\text{l}$  of the  $\text{Ru}(\text{bpy}-\text{Me}_2)_2(\text{bpy}-(\text{COOH})_2)^{2+}$  solution was added to the EDC solution and then placed dropwise onto the silanized PtSi surface for 2 h. Afterwards, the chip was soaked in phosphate buffer for 24 h and then rinsed with Milli-Q water and dried with high-pressure nitrogen. As a control, unmodified PtSi also underwent the same treatment. For ECL detection of single-strand DNA labeled with  $\text{Ru}(\text{bpy})_3^{2+}$ , a 10 bp sequence containing a 3'-ribo-U, 3'-ribo-U-TTTCAGG-CAT- $\text{Ru}(\text{bpy})_3^{2+}$ , was synthesized using an automated DNA synthesizer (Applied Biosystems, Foster City, CA). The phosphoramidite containing  $\text{Ru}(\text{bpy})_3^{2+}$  was provided by IGEN, Inc. (Gaithersburg, MD). To allow covalent attachment to the aminosilane on the PtSi surface, the 3'-ribo-U was oxidized to the dialdehyde by placing 50  $\mu\text{l}$  of approximately 400  $\mu\text{M}$  solution of DNA in water with 100  $\mu\text{l}$  or 0.2 M sodium acetate (pH 5.2; EM Sciences) and 50  $\mu\text{l}$  or 0.1 M sodium metaperiodate ( $\text{NaIO}_4$ ; Pierce) in Milli-Q water. The mixture was incubated at RT for 40 min and then desalted by passing through a G25 Sephadex (Sigma, St. Louis, MO) column and dried by evaporation. The resulting 3'-dialdehyde was then covalently attached to the surface amines using a Schiff's base reaction and following reduction of the resulting imine by sodium cyanoborohydride. This was accomplished by dissolving the DNA into 0.3 M sodium borate buffer (pH 9.0) containing 0.2 M sodium cyanoborohydride ( $\text{NaCNBH}_4$ ; Aldrich) at a final concentration of 500 nM. The mixture was placed onto the silanized PtSi surface and allowed to incubate at room temperature for 1 h. The surface was then rinsed with phosphate buffer and Milli-Q water and then dried with high-pressure nitrogen. The PtSi chip was then mounted into the same cell used in the above electrochemical measurements. ECL and voltammetry were then obtained using 0.1 M

phosphate buffer (pH 7.5) containing 0.1 M tri-*n*-propylamine (TPrA; Aldrich).

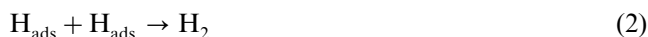
### 3. Results and discussion

#### 3.1. Underpotential deposition of hydrogen and copper on PtSi surfaces

One way of determining the stability of the PtSi surface after a variety of chemical pretreatments as well as upon extensive potential cycling in aqueous solution is to evaluate the electrochemistry of a redox couple that depends highly on the structure and composition of the electrode surface. For this purpose, we chose the upd of protons in the her and the upd of copper(II) ions. In the her, the overall mechanism on polycrystalline platinum is believed to involve three steps [33–36]. The first step, which is most critical in our evaluation of the PtSi surface, is called the initial discharge step [33,34]. This step occurs at potentials slightly more positive than the bulk reduction of hydrogen and involves the simultaneous reduction and adsorption of hydrogen onto the platinum surface,



This initial step is followed by either a chemical recombination step where two adsorbed hydrogen radicals combine to form dihydrogen [33–36],



or an electrochemical desorption step, which involves the reduction of a second proton, and then desorption of dihydrogen [33–36].



As one would expect, the reduction and adsorption of protons onto platinum in the initial discharge step is highly dependent upon the crystal structure and cleanliness of the platinum surface; therefore, the upd of hydrogen in the her is a good diagnostic for detection of the presence of polycrystalline platinum domains on the surface of PtSi.

Fig. 2 shows cyclic voltammograms obtained in 1.0 M H<sub>2</sub>SO<sub>4</sub> at a number of pretreated PtSi surfaces and at a mechanically polished platinum disk electrode. The voltammogram shown in Fig. 2e exhibits the electrochemical behavior expected for a clean polycrystalline platinum surface in the absence of oxygen [33–36]. The reduction of protons (H<sup>+</sup>) and corresponding oxidation of hydrogen (H<sub>2</sub>), which is evident by the small peak observed upon switching the potential positive, is observed at potentials more negative than –0.2 V versus Ag | AgCl | KCl (sat.). Additionally, three upd waves are observed between 0.1 and –0.2 V versus Ag | AgCl | KCl (sat.); at potentials somewhat more

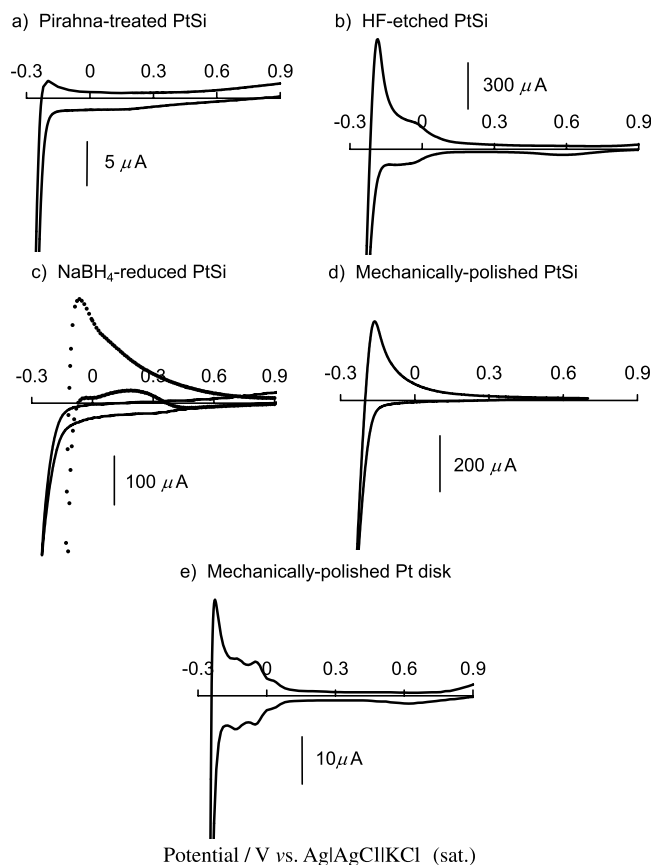


Fig. 2. Cyclic voltammograms involving the her in 1.0 M H<sub>2</sub>SO<sub>4</sub> and at a scan rate of 0.1 V s<sup>-1</sup> at PtSi surfaces (area = 0.071 cm<sup>2</sup>) pretreated by (a) exposure to piranha, (b) exposure to 1% HF, (c) exposure to 1 M NaBH<sub>4</sub>, before (dotted line) and after (solid line) numerous cycles, and (d) mechanically polished.

positive than the reduction of protons in solution to H<sub>2</sub>. Upon comparison to the voltammograms obtained at each of the PtSi surfaces, only the HF-etched surface (voltammogram in Fig. 2b) exhibited similar behavior, substantiating the presence of bulk polycrystalline platinum domains on this surface. One other observation to note is the presence of hydrogen oxidation on a mechanically polished PtSi surface (Fig. 2d). Previous studies performed on Pt have suggested that the occurrence of this reaction also require polycrystalline platinum domains. However, if these domains were present on this particular PtSi surface, then upd of hydrogen should also have been observed, but this is not the case [33–36]. As shown in Fig. 2d, no surface oxidation or reduction waves between 0.1 and –0.2 V versus Ag | AgCl | KCl (sat.) were observed. This suggests that there may be another mechanism for the oxidation of hydrogen that does not require the adsorption onto adjacent platinum atoms on the surface. A future investigation into the mechanism for her will be performed using SECM.

As with proton reduction, studies performed on the upd of copper(II) ions (Cu<sup>2+</sup>) on a multitude of

crystalline Pt surfaces have shown that copper upd requires f.c.c. and h.c.p. threefold hollow sites, so, as with proton adsorption, polycrystalline platinum domains are needed to facilitate upd [37–39]. Fig. 3 shows the deposition and bulk reduction of  $\text{Cu}^{2+}$  in 0.2 M  $\text{H}_2\text{SO}_4$  at a number of PtSi surfaces with different pretreatments, as well as at a mechanically polished Pt disk electrode. As expected, voltammetry obtained on a polycrystalline platinum disk electrode (Fig. 3d) exhibits bulk deposition of  $\text{Cu}^{2+}$  ions at potentials more negative than 0 V versus  $\text{Ag}|\text{AgCl}|\text{KCl}(\text{sat.})$  and the corresponding stripping wave (large symmetric oxidation wave) at +0.1 V versus  $\text{Ag}|\text{AgCl}|\text{KCl}(\text{sat.})$  [37–39]. Additionally, the oxidation and reduction waves obtained between 0.6 and 0.2 V versus  $\text{Ag}|\text{AgCl}|\text{KCl}(\text{sat.})$  reach a plateau at concentrations equal to and greater than 2 mM  $\text{Cu}^{2+}$ . The presence of such a plateau is indicative of upd copper ions where only monolayers of copper can be deposited onto the surface [37,38]. This is in direct contrast to the contin-

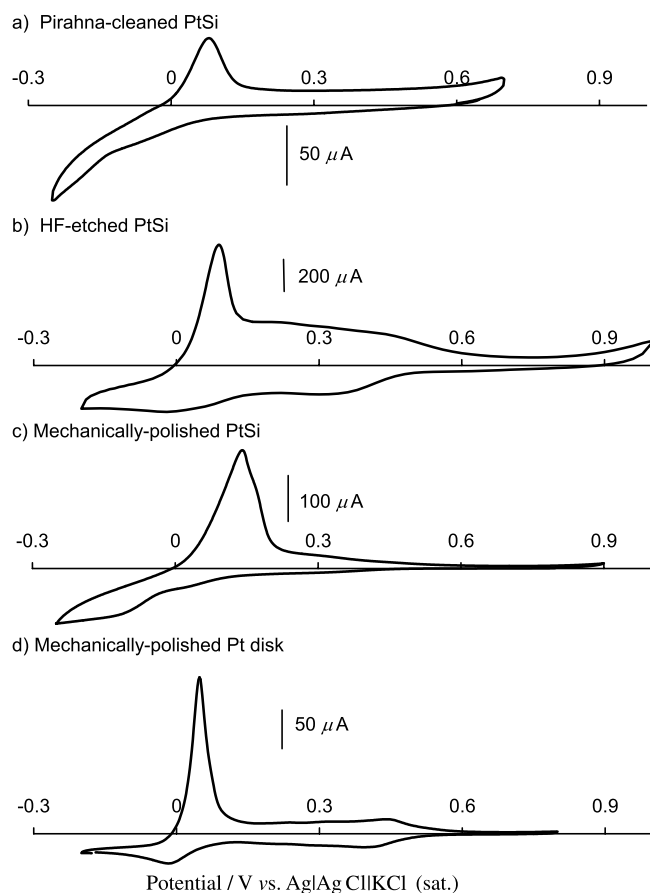


Fig. 3. Cyclic voltammograms of the deposition of copper at PtSi surfaces (area = 0.071 cm<sup>2</sup>) pretreated by (a) exposure to piranha, (b) exposure to 1% HF and (c) mechanically polished, and (d) at a mechanically polished Pt disk electrode. All voltammograms were obtained in 0.2 M  $\text{H}_2\text{SO}_4$  containing 20 mM  $\text{CuSO}_4$  and at a scan rate of 0.1 V s<sup>-1</sup>.

uous increase in current observed with the bulk reduction of copper on platinum at 0.1 V versus  $\text{Ag}|\text{AgCl}|\text{KCl}(\text{sat.})$ . Upon comparing this electrochemical behavior to the other pretreated PtSi surfaces, the bulk reduction and corresponding stripping wave was observed on all of the PtSi surfaces; however, only the HF-etched PtSi surface, as shown in Fig. 2b, clearly exhibited waves attributable to the upd of copper(II) ions. A small amount of upd of copper may be also observed at the mechanically polished PtSi, as is evident from the small increase in the current between 0.5 and 0.2 V versus  $\text{Ag}|\text{AgCl}|\text{KCl}(\text{sat.})$  but not as evident as on the HF-treated surface. Along with our previous results involving the upd of hydrogen, the HF-etched PtSi surface appears to be the only treated PtSi surface that contains domains of polycrystalline platinum.

### 3.2. Heterogeneous electron transfer behavior at PtSi surfaces

The voltammetry of both positively and negatively charged redox couples were used to evaluate the rate of heterogeneous electron transfer at each of the chemically treated, as well as at the mechanically polished, PtSi surfaces. These couples included hexaamineruthenium(III)chloride ( $\text{Ru}(\text{NH}_3)_6\text{Cl}_3$ ), potassium ferricyanide ( $\text{K}_3\text{Fe}(\text{CN})_6$ ), potassium hexacyanoruthenium(II) hydrate ( $\text{K}_4\text{Ru}(\text{CN})_6$ ) and tris(2,2'-bipyridyl)ruthenium(II) dichloride hexahydrate ( $\text{Ru}(\text{bpy})_3\text{Cl}_2$ ). All four couples have relatively fast rates of electron transfer at a clean platinum electrode and exhibit reversible (or Nernstian) electrochemical behavior as is evident from the anodic peak current equaling the cathodic peak current ( $I_{\text{pa}} = I_{\text{pc}}$ ) and by the potential difference between the peaks ( $\Delta E_{\text{p}} = E_{\text{pa}} - E_{\text{pc}}$ ) being approximately 59 mV for a single electron transfer ( $n = 1$ ) [40].

Fig. 4 shows the cyclic voltammograms of the negative redox couple,  $\text{K}_3\text{Fe}(\text{CN})_6$ , while Fig. 5 shows the cyclic voltammogram of the positive redox couple,  $\text{Ru}(\text{NH}_3)_6\text{Cl}_3$ , obtained at PtSi surfaces after being treated with piranha solution (a), HF (b),  $\text{NaBH}_4$  (c), and upon mechanical polishing (d). Although not shown, two additional redox couples were evaluated: the negative redox couple,  $\text{K}_4\text{Ru}(\text{CN})_6$ , and the positive redox couple,  $\text{Ru}(\text{bpy})_3\text{Cl}_2$ . The voltammograms for  $\text{K}_4\text{Ru}(\text{CN})_6$  on each of these surfaces were similar to those obtained for  $\text{K}_3\text{Fe}(\text{CN})_6$  (Fig. 4) while the voltammograms for  $\text{Ru}(\text{bpy})_3\text{Cl}_2$  were similar to  $\text{Ru}(\text{NH}_3)_6\text{Cl}_3$  (Fig. 5). Along with these figures, Table 1 lists the peak separations ( $\Delta E_{\text{p}}$ ) observed for each of the couples at all four of the PtSi surfaces investigated.

Upon comparing Fig. 4 with Fig. 5, the greatest difference in the voltammograms was observed on PtSi surfaces that had been exposed to only piranha solution. Along with the information provided in Table 1, the peak separation for the negative redox couple,

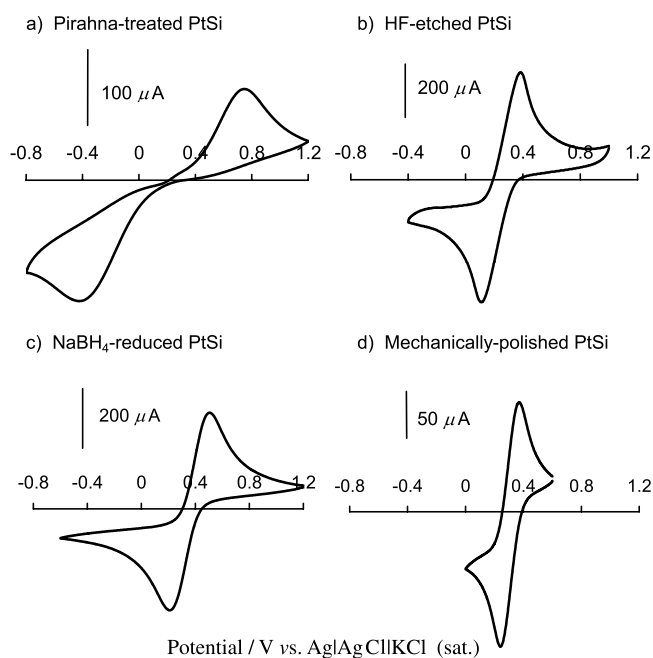


Fig. 4. Cyclic voltammograms of 10 mM  $\text{K}_3\text{Fe}(\text{CN})_6$  in 0.1 M KCl at PtSi surfaces (area =  $0.071 \text{ cm}^2$ ) pretreated by (a) exposure to piranha, (b) exposure to 1% HF, and (c) exposure to 1.0 M  $\text{NaBH}_4$ . Cyclic voltammogram of 4.4 mM  $\text{K}_3\text{Fe}(\text{CN})_6$  at (d) a mechanically polished PtSi surface (area =  $0.031 \text{ cm}^2$ ) at a scan rate of  $0.1 \text{ V s}^{-1}$ .

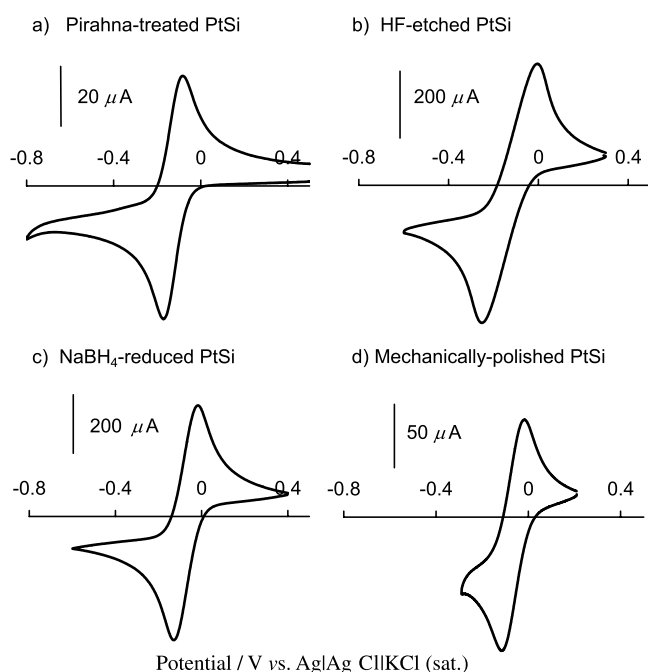


Fig. 5. Cyclic voltammograms of 10 mM  $\text{Ru}(\text{NH}_3)_6\text{Cl}_3$  in 0.1 M KCl at PtSi surfaces (area =  $0.071 \text{ cm}^2$ ) pretreated by (a) exposure to piranha, (b) exposure to 1% HF, and (c) exposure to 1.0 M  $\text{NaBH}_4$ . Cyclic voltammogram of 3.3 mM  $\text{Ru}(\text{NH}_3)_6\text{Cl}_3$  obtained at (d) a mechanically polished PtSi surface (area =  $0.031 \text{ cm}^2$ ) and at a scan rate of  $0.1 \text{ V s}^{-1}$ .

$\text{K}_3\text{Fe}(\text{CN})_6$ , is considerably larger than the peak separation observed for the positive redox couple,

$\text{Ru}(\text{NH}_3)_6\text{Cl}_3$ . Additionally, while the anodic peak current was equal to the cathodic peak currents for positive redox couples, this was not the case for the negative redox couples. The large peak separation for the negative redox couples suggests a considerably slower rate of heterogeneous electron for these couples when compared with the positive redox couples. In direct contrast, the only PtSi surface that came close to exhibiting Nernstian behavior with peak separations approaching 59 mV was the mechanically polished surface, which had peak separations ranging from approximately 70 to 110 mV. Finally, as shown in Figs. 2–5, the voltammetric peak currents increased upon the removal of the oxide layer either by exposure of the PtSi surface to the etchant, HF or by mechanically polishing the surface. Such an increase in current suggests an increase in the electrochemically active surface area upon removal of this oxide layer.

Based on the above voltammetric results, the sluggish electron transfer of the negative redox couples appears to be directly associated with the amount of the oxide layer on the PtSi surface, with the surface exposed to piranha solution, a strong oxidant, having the slowest rate. One possible explanation for this behavior is that a Frumkin or potential field effect exists due to the presence of the negative oxide layer at the electrode surface. This layer can potentially interfere with the ability of the negative redox couple to approach the surface requiring a greater driving voltage to facilitate electron transfer [40]. Similar behavior has been observed at glassy carbon electrodes modified with 4-aminobenzoic acid where the presence of surface carboxylates significantly decreased the rate of electron transfer of  $\text{K}_3\text{Fe}(\text{CN})_6$  [41]. High concentrations of ions in the electrolyte solution, however, should minimize this effect. Another plausible reason for this effect is that the electrode surface is being blocked by a species that forms an insoluble film during oxidation and reduction. Previous studies involving the electrochemistry and spectroscopy of  $\text{Fe}(\text{CN})_6^{3-/4-}$  have confirmed precipitation of an insoluble material onto the electrode surface upon the oxidation of  $\text{Fe}(\text{CN})_6^{4-}$  [42–45]. This precipitate, which is dependent upon the cation present in the electrolyte as well as the electrode size, has been shown to slowdown the rate of electron transfer. One contradiction to this explanation, however, is that similar behavior was also observed for  $\text{Ru}(\text{CN})_6^{3-/4-}$  which, so far, has not been shown to form an insoluble film upon reduction.

In an attempt to clarify the reason for the sluggish electron transfer of negative redox couples at the piranha-exposed PtSi, the oxidation of ferrocene dicarboxylate, where the charge on the redox couple goes from  $-2$  to  $-1$ , and the reduction of potassium hexachloroiridate ( $\text{K}_2\text{IrCl}_6$ ), where the redox couple charge goes from a  $-2$  to a  $-3$ , was also investigated at

Table 1

Peak separation ( $\Delta E_p$ ) measure at a scan rate of  $0.1 \text{ V s}^{-1}$  for both positively charged and negatively charged redox couples on PtSi surfaces after different pretreatments

Pretreatments used prior to measurement	Peak separation for the following redox couples/V			
	$\text{Fe}(\text{CN})_6^{3-}$	$\text{Ru}(\text{CN})_6^{4-}$	$\text{Ru}(\text{NH}_3)_6^{3+}$	$\text{Ru}(\text{bpy})_3^{2+}$
Piranha	1.15	1.55	0.089–0.095	0.103
HF-etched	0.288	0.214	0.154	0.104
$\text{NaBH}_4$ -reduced	0.323	N/A	0.098–0.112	0.092
Mechanically polished	0.108	N/A	0.099	0.070

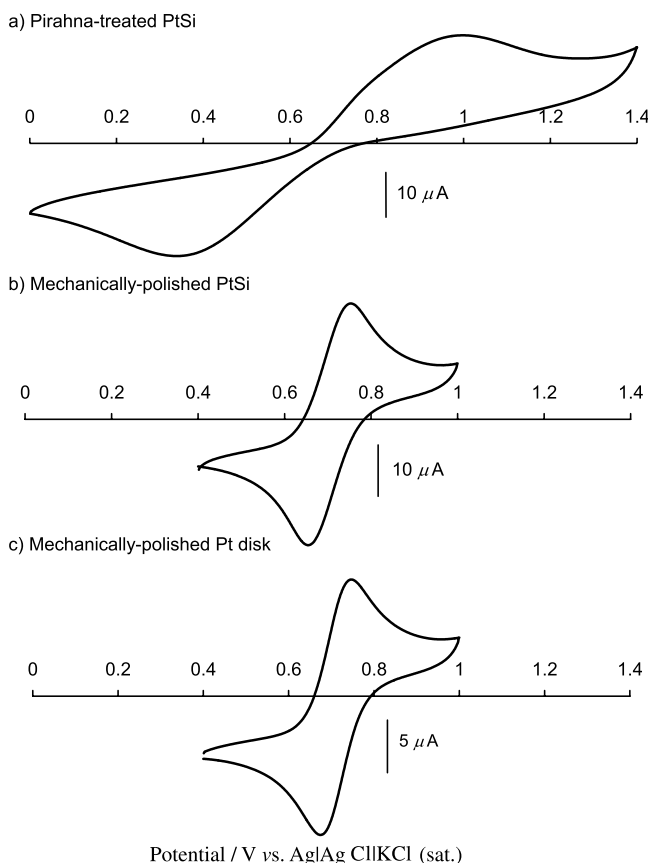


Fig. 6. Cyclic voltammograms of  $2.7 \text{ mM K}_2\text{IrCl}_6$  in  $0.1 \text{ M KCl}$  at PtSi surfaces (area =  $0.031 \text{ cm}^2$ ) pretreated by (a) exposure to piranha and (b) mechanically polished. Cyclic voltammogram of the same solution at (c) a mechanically polished Pt disk (area =  $0.0080 \text{ cm}^2$ ). All scan rates were  $0.1 \text{ V s}^{-1}$ .

this surface. The cyclic voltammograms of these two redox couples are presented in Figs. 6 and 7. For  $\text{K}_2\text{IrCl}_6$ , peak analysis of the voltammogram at the piranha-treated PtSi indicated a peak separation of 604 mV. This value is still considerably larger than that observed for the peak separation of the positive redox couple but smaller than the peak separation observed for the  $-3/-4$  redox couples. In addition, Fig. 6 also shows the voltammograms obtained at a mechanically polished PtSi surface and a mechanically polished Pt disk electrode. As seen in previous scans on these

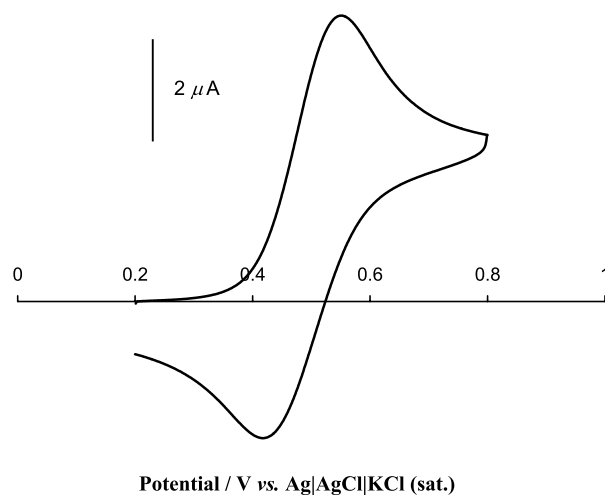


Fig. 7. Cyclic voltammogram of a saturated solution ( $<1 \text{ mM}$ ) of ferrocene dicarboxylate in  $0.2 \text{ M NaCl}$  at a PtSi surface (area =  $0.031 \text{ cm}^2$ ) pretreated by exposure to piranha. Scan rate is  $0.1 \text{ V s}^{-1}$ .

surfaces, the peak separations are considerably smaller: 100 mV on the polished PtSi and 72 mV on the clean Pt disk electrode. As the negative charge on the redox couple was decreased further, an even smaller peak separation of 96 mV was observed as shown by the voltammogram of ferrocene dicarboxylate in Fig. 7. This value is comparable to peak separations observed for the positive redox couples,  $\text{Ru}(\text{NH}_3)_6^{3+}$  and  $\text{Ru}(\text{bpy})_3^{2+}$ . Based on this result, the sluggish electron transfer that is observed on a piranha-treated PtSi surface does appear to be associated with the magnitude of negative charge on the redox couple. Whether this sluggish electron transfer is due to a Frumkin effect or the formation of an insoluble film, or another effect, is still unclear.

### 3.3. Rate of electron transfer by SECM

Although the peak separation obtained by CV provided a qualitative evaluation of the heterogeneous rates of electron transfer, SECM is more accurate in determining a quantitative rate of heterogeneous electron transfer for a quasi-reversible electrochemical reaction at the surface [46,47]. Fig. 8 shows the experimental as well as the theoretical approach curves

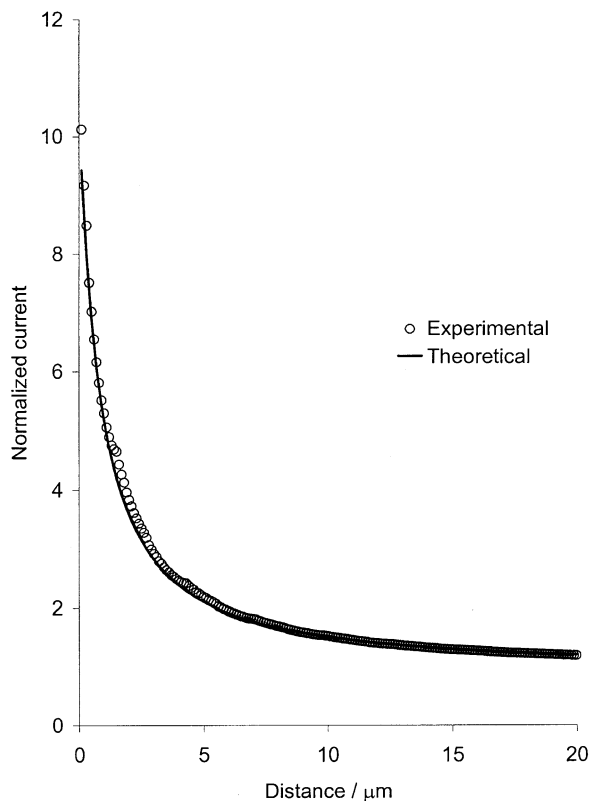


Fig. 8. SECM approach curve for 1 mM  $\text{Ru}(\text{NH}_3)_6\text{Cl}_3$  in 0.2 M NaCl with the tip potential biased on  $-0.28$  V vs.  $\text{Ag} | \text{AgCl} | \text{KCl}$  (sat.) and the substrate potential biased at  $0.1$  V vs.  $\text{Ag} | \text{AgCl}$ . Approach rate was  $3 \mu\text{m s}^{-1}$ .

for  $\text{Ru}(\text{NH}_3)_6^{3+}$  at a PtSi surface that was exposed to piranha solution prior to the SECM measurement. In this case, the tip potential was held at  $-0.28$  V versus  $\text{Ag} | \text{AgCl} | \text{KCl}$  (sat.) while the substrate was biased at a potential of  $0.1$  V versus  $\text{Ag} | \text{AgCl} | \text{KCl}$  (sat.) corresponding to an overpotential of  $0.260$  V. As Fig. 8 shows, the experimental curves agree well with the diffusion-controlled theoretical fit indicating a fast rate of electron transfer for  $\text{Ru}(\text{NH}_3)_6^{3+}$  at this surface. Even as the potential approached  $E^\circ$  ( $-0.16$  V versus  $\text{Ag} | \text{AgCl} | \text{KCl}$  (sat.)), diffusion-controlled positive feedback was still observed. This was not the case for  $\text{Fe}(\text{CN})_6^{3-}$ . Fig. 9a shows the experimental as well as the theoretical approach curves for this redox couple at the same PtSi surface. The most noticeable difference is that negative feedback is now observed at a potential of  $0.8$  V versus  $\text{Ag} | \text{AgCl} | \text{KCl}$  (sat.), which corresponds to an overpotential of  $0.58$  V. Even at a potential of  $1.1$  V versus  $\text{Ag} | \text{AgCl} | \text{KCl}$  (sat.) where positive feedback is observed, the normalized current is considerably lower than that observed for  $\text{Ru}(\text{NH}_3)_6^{3+}$ . This behavior confirms a kinetic-controlled mechanism instead of a diffusion-controlled mechanism. From the theoretical fits given in Fig. 9a, the potential-dependent rate constant,  $k_f$ , was determined for each substrate potential

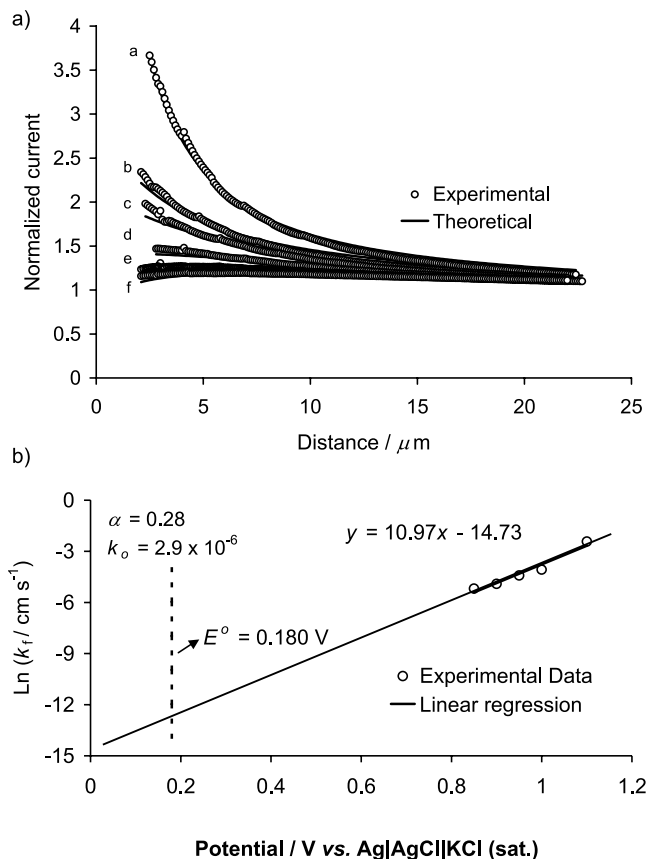


Fig. 9. (a) SECM approach curves for 1 mM  $\text{K}_3\text{Fe}(\text{CN})_6$  in 0.1 M NaCl with the tip potential set at  $0$  V vs.  $\text{Ag} | \text{AgCl} | \text{KCl}$  (sat.) and the substrate set at  $1.1$  V (a),  $1.0$  V (b),  $0.95$  V (c),  $0.9$  V (d),  $0.85$  V (e), and  $0.8$  V (f) vs.  $\text{Ag} | \text{AgCl} | \text{KCl}$  (sat.). Approach rate was  $3 \mu\text{m s}^{-1}$ . (b) Plot of the natural log of the potential-dependent rate constant ( $k_f$ ) as a function of substrate potential.

and the natural log of this rate constant plotted as a function of the substrate potential. This plot is given in Fig. 9b. A linear response was observed with a slope of  $10.97 \text{ V}^{-1}$  and an intercept of  $-14.7$  at the  $E^\circ$  of  $0.180$  V versus  $\text{Ag} | \text{AgCl} | \text{KCl}$  (sat.). From the Butler–Volmer relation, a transfer coefficient ( $\alpha$ ) of  $0.28$  and a standard rate constant ( $k^\circ$ ) of  $2.9 \times 10^{-6} \text{ cm s}^{-1}$  were determined. This is considerably slower than the standard rate constant of  $0.1 \text{ cm s}^{-1}$  reported at clean platinum electrodes [42]. Overall, the quantitative rate of electron transfer as determined by SECM agrees well with that estimated from the peak separation observed in the CV. Based on these results, the electron transfer rate of the positive redox couples appears to be considerably faster than the more negatively charged redox couples on this surface.

#### 3.4. Surface analysis of piranha-treated PtSi surfaces

As the above results indicate, the sluggish rate of electron transfer of the negative redox couples appears to be associated with an oxide layer on the PtSi. To

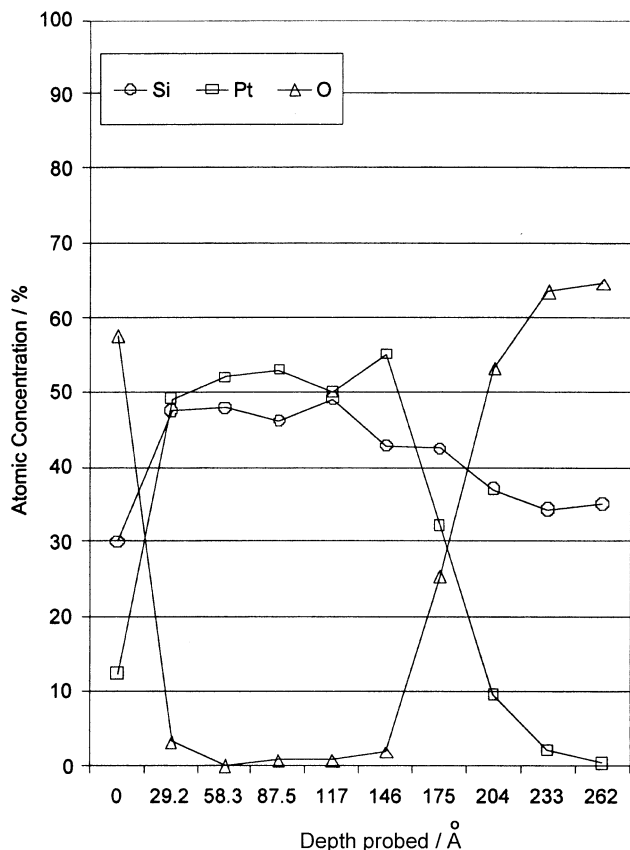


Fig. 10. Depth profile showing the atomic concentrations of Pt, Si and O as a function of depth probed (Å) on PtSi after exposure to piranha.

confirm the presence of silicon oxide, which could be used for covalent attachment of ECL labels to the surface, a depth profile of the PtSi layer as well as the atomic concentrations of the surface elements were obtained using high-resolution XPS. Fig. 10 shows the concentrations of platinum, silicon, and oxygen in atom percentages as a function of the distance (Å) probed into a PtSi sample that was pretreated with piranha. While the first layers contain  $\text{PtSi}_2\text{O}_4$ , the underlying PtSi layers appear to show a Pt:Si 1:1 ratio down to 146 Å. These results, which show a higher percentage of silicon on the surface and a 1:1 Pt to Si ratio below the surface, agree with previously reported surface analyses [16,48,49]. In addition to the depth profiling, a high-resolution surface scan was performed after different pretreatments to evaluate the atomic concentrations of Pt, Si and O on each of these PtSi surfaces. These concentrations were determined by integrating the peak area for Pt 4f at a binding energy of 68–88 eV, Si 2p at a binding energy of 145–165 eV and O 1s at a binding energy of 525–545 eV and are given in Table 2. The HF-etched surface, which showed a mole ratio for the three components of  $\text{Pt}_4\text{SiO}_2$ , had the highest amount of Pt on the surface, while the mechanically polished surface, which showed a mole ratio of  $\text{PtSiO}_2$ , was the only

Table 2

Atomic concentrations on the surface of different pretreated PtSi by high-resolution XPS

Chemical pretreatments	Atomic concentration/%		
	Pt1 (68–88 eV)	Si2 (145–165 eV)	O1 (525–545 eV)
Piranha	15	27	58
$\text{NaBH}_4$	16	25	59
HF-etched	54	14	32
Mechanically polished	29	25	46

Binding energies (eV) used for the analysis are provided in parentheses after the atom.

surface that exhibited a 1:1 Pt to Si ratio. The piranha- and borohydride-treated surfaces showed almost the same composition and agree with the atomic concentrations measured on the surface of different samples analyzed during the depth profiling. Based on the electrochemical results, one would expect the  $\text{NaBH}_4$ -treated surface to have less oxygen than the piranha-treated surface. However, these samples were exposed to air prior to the XPS measurement and so the  $\text{NaBH}_4$ -treated surface may have undergone further oxidation before analysis. This may also be the case for the mechanically polished PtSi, which also contained an unexpectedly high amount of surface oxide.

### 3.5. Topography and localized conductivity by AFM

As the above studies show, the presence of an oxide layer on the PtSi surface still allows the transfer electrons although at a higher overpotential. One question that remains is whether electron transfer occurs across the whole surface through tunneling or only at localized domains. Although SECM can be used to map areas of electron transfer at interfaces, the resolution with the tip used to obtain the approach curves was not high enough to determine whether there were localized regions of electron transfer on this surface. An alternative was to use AFM modified with a conductive tip to measure the variation in film conductivity over sub-micron length scales by monitoring the current flow from the conductive tip to the PtSi film during an applied d.c. bias. Fig. 11 shows the surface topography (a) and conductivity (b) images obtained for a PtSi film exposed to piranha. In agreement with previous studies, the AFM topography (Fig. 11a) shows that the PtSi coating is fairly smooth ( $\sim 1.3$  nm root mean-square (RMS) surface roughness) but non-uniformly distributed. The presence of small pinhole-like topographic defects, approximately 20 nm in diameter, are observed between the larger PtSi grains. Comparison of the simultaneously acquired topography (Fig. 11a) and

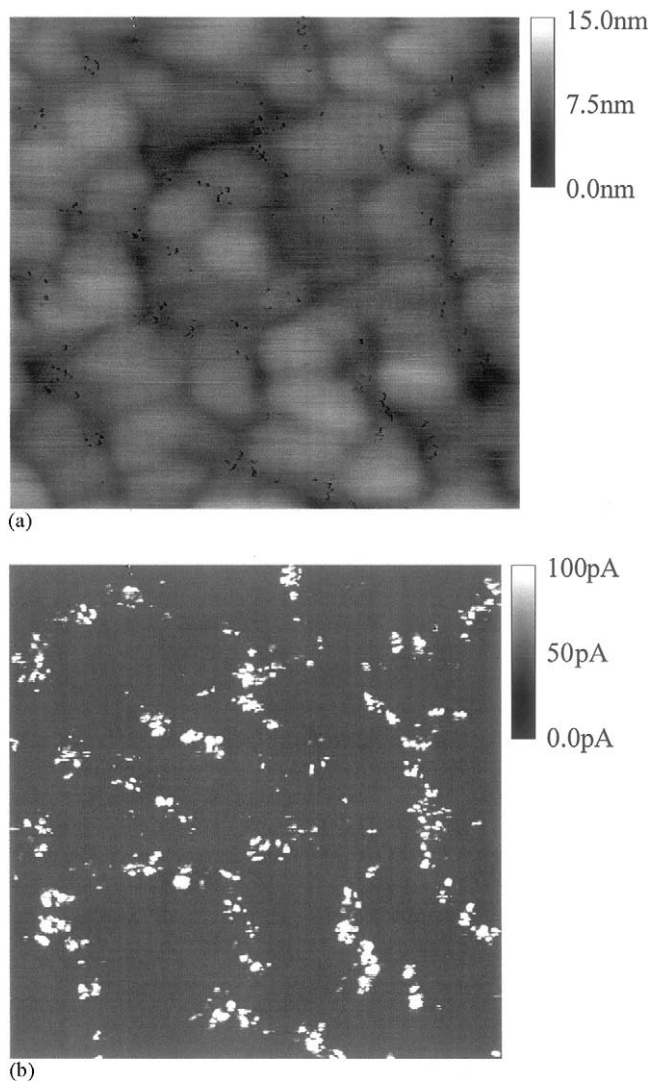


Fig. 11. AFM images ( $1.0 \mu\text{m} \times 1.0 \mu\text{m}$ ) showing measured (a) topography and (b) conductivity acquired at a PtSi electrode after piranha treatment.

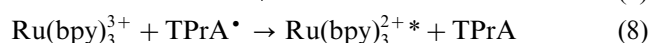
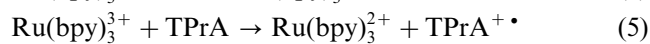
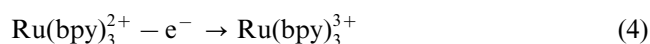
conductivity image (Fig. 11b) indicates that these pin-hole-like areas correlate with the more conductive regions (brighter areas in Fig. 11b) on the surface. This observation suggests that the oxide layer resides mainly on the surface of the PtSi grains and that the smaller peak currents observed in the voltammograms obtained on the PtSi pretreated with piranha is due to a smaller active electrode area which can increase upon the removal of the oxide layer by exposure to HF or through mechanical polishing.

### 3.6. ECL on PtSi surfaces

As shown above, an oxidized PtSi surface still facilitates the relatively fast electron transfer of positive redox couples; therefore, one should be able to generate ECL of  $\text{Ru}(\text{bpy})_3^{2+}$  at this surface. In the next set of

experiments, we investigated the ability to produce ECL at a PtSi surface that has the ECL label,  $\text{Ru}(\text{bpy})_3^{2+}$ , attached to the oxide layer on the PtSi grains. In one case, this label was  $\text{Ru}(\text{bpy}-\text{Me}_2)_2(\text{bpy}-(\text{COOH})_2)^{2+}$  while in the other was a  $\text{Ru}(\text{bpy})_3^{2+}$  labeled single strand of DNA (ssDNA) consisting of 10 bases (or 10-mer). The attachment of both species was achieved by first functionalizing the surface with an aminosilane. The details and procedure for these attachments are provided in Section 2.

To generate ECL under aqueous conditions, the co-reactant, tri-*n*-propylamine (TPrA), was added to the phosphate buffer solution that was used as the electrolyte for these measurements. The mechanism resulting in the light emitting excited state of  $\text{Ru}(\text{bpy})_3^{2+}$  is as follows:



The current from the electrode reaction and the corresponding PMT current (light emission) for  $\text{Ru}(\text{bpy})_3^{2+}$  at both an unmodified PtSi and PtSi surfaces silanized with either (4-aminobutyl)-dimethylmethoxysilane and (3-aminopropyl)-trimethoxysilane are given in Fig. 12. The voltammogram in Fig. 12a is representative of the results that are observed at each of the PtSi surfaces containing surface bound  $\text{Ru}(\text{bpy}-\text{Me}_2)_2(\text{bpy}-(\text{COOH})_2)^{2+}$ . The increase in electrochemical current (bottom curve) at potentials greater than 0.8 V versus  $\text{Ag} | \text{AgCl} | \text{KCl} (\text{sat.})$  is due to the oxidation of the co-reactant, TPrA. Emission, as is evident from the increase in PMT current (top curve), is not observed until  $\text{Ru}(\text{bpy})_3^{2+}$  is oxidized to the 3+ state at potentials greater than 1.2 V versus  $\text{Ag} | \text{AgCl} | \text{KCl} (\text{sat.})$ . This behavior agrees with previous experiments involving ECL of surface bound  $\text{Ru}(\text{bpy})_3^{2+}$  in the presence of TPrA [50,51]. As is shown in Fig. 12b, the highest signals were observed at surfaces modified with (4-aminobutyl)-dimethylmethoxysilane while the smallest signals were observed at surfaces modified with (3-aminopropyl)-trimethoxysilane. We suspect that the moderate signal observed at the unmodified PtSi is most likely due to  $\text{Ru}(\text{bpy})_3^{2+}$  that is non-specifically adsorbed to the oxidized surface. Similar behavior has also been seen at the surfaces of other electrodes [50]. Additionally, the lower signals at the (3-aminopropyl)-trimethoxysilane-modified PtSi surface suggests extensive cross-linking between surface bound methoxysilanes which blocks the oxidation of both TPrA and  $\text{Ru}(\text{bpy})_3^{2+}$ . Based on these results, (4-aminobutyl)-dimethylmethoxysilane was used for all additional ECL experiments on PtSi.

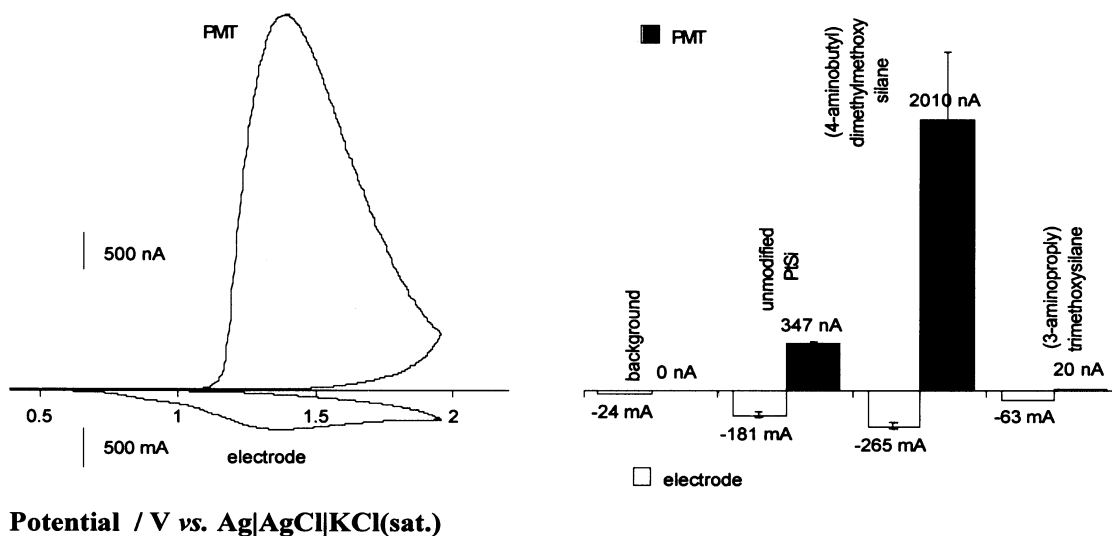


Fig. 12. (a) Potential scan of electrode current (bottom curve) and PMT (top curve) current with  $\text{Ru}(\text{bpy}-\text{Me}_2)_2(\text{bpy}-(\text{COOH})_2)^{2+}$  on PtSi surfaces silanized with (4-aminobutyl)-dimethylmethoxysilane obtained in 0.1 M phosphate buffer (pH 7.4) containing 0.1 M TPrA and at a scan rate of  $0.05 \text{ V s}^{-1}$ . (b) Average maximum current ( $n = 3$ ) for  $\text{Ru}(\text{bpy}-\text{Me}_2)_2(\text{bpy}-(\text{COOH})_2)^{2+}$  obtained of background and of different PtSi surfaces.

The next logical step was to examine the detection of  $\text{Ru}(\text{bpy})_3^{2+}$  that was linked onto the 5'-end of a single strand of DNA which, in turn, was bound to the surface of the PtSi through the 3'-end. The details behind the chemistry and the actual procedures used are provided in Section 2. Fig. 13 shows the electrochemical and emission response for ssDNA labeled with  $\text{Ru}(\text{bpy})_3^{2+}$  on a PtSi surface that was left unmodified and modified with (4-aminobutyl)-dimethylmethoxysilane. When the emission from the non-specific background obtained at the unmodified surface is compared with the emission from the PtSi surface modified for attachment chemistry (Fig. 13b), a onefold increase in the signal is observed for the attached DNA. This, we feel, demonstrates the viability of using PtSi as a substrate for electrode arrays used for the electrochemical detection of surface bound biomolecules.

#### 4. Conclusions

Electrochemical methods and surface techniques, including conductive AFM and XPS, were applied to characterize the electrochemical behavior of PtSi surfaces that were pretreated using a variety of protocols. Based on the voltammetric and SECM results, PtSi surfaces pretreated with piranha exhibited considerably slower rates of heterogeneous electron transfer for negatively charged redox couples, such as  $\text{K}_2\text{IrCl}_6$ ,  $\text{K}_3\text{Fe}(\text{CN})_6$ , and  $\text{K}_3\text{Ru}(\text{CN})_6$ . These rates appeared to decrease correspondingly with the magnitude of the negative charge. Surface analysis and depth profiles obtained using AES showed that PtSi surfaces pretreated with piranha contained surface oxides. Removal of surface oxides upon exposure to HF acid not only

increase the electrochemical active area of the surface but also increase the rate of electron transfer of the

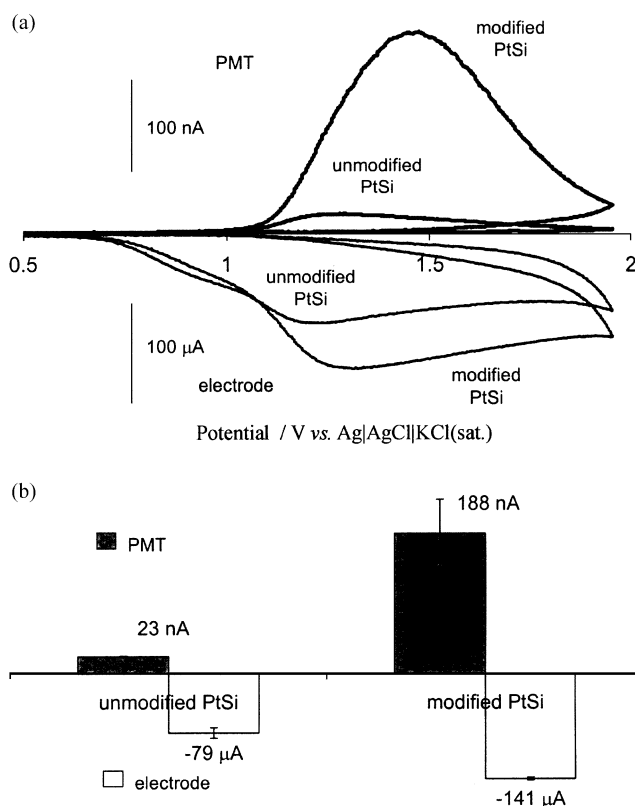


Fig. 13. (a) Potential scan of electrode current (bottom curve) and PMT current (top curve) of  $\text{Ru}(\text{bpy})_3^{2+}$ -labeled DNA on unmodified PtSi and on a PtSi surface modified with (4-aminobutyl)-dimethylmethoxysilane. Scan was obtained in 0.1 M phosphate buffer (pH 7.4) containing 0.1 M TPrA and at a scan rate  $0.05 \text{ V s}^{-1}$ . (b) Average maximum current ( $n = 3$ ) obtained of  $\text{Ru}(\text{bpy})_3^{2+}$ -labeled ssDNA at unmodified and modified PtSi surfaces.

negative redox couples. Furthermore, the upd of both protons and copper(II) ions also confirmed the presence of polycrystalline platinum domains on the surface of the PtSi after exposure to HF. AFM with a conductive tip to study the topography along with the localized surface conductivity showed that, in the presence of this oxide layer, electron transfer occurs at nanoscale domains located between PtSi grains. As a result of these properties, we were able to generate ECL from Ru(bpy)<sub>3</sub><sup>2+</sup> bound to the oxidized PtSi surface demonstrating the feasibility of using this surface as a platform for chemical and biological assays that use electrochemical detection.

### Acknowledgements

Support from the National Science Foundation (CHE9876855) is greatly appreciated.

### References

- [1] M.P. Lepselter, S.M. Sze, *Bell Syst. Tech. J.* 47 (1968) 195.
- [2] M.P. Lepselter, J.M. Andrews, in: B. Schwartz (Ed.), *The Electrochemical Society Softbound Symposium Series*, New York, 1969, p. 159.
- [3] A.H. Huchberg, *Transactions: Electronic Materials Processing Conference*, Materials Research Corp, Orangeburg, NY, 1973, p. 81.
- [4] S.P. Murarka, *J. Vac. Sci. Technol.* 17 (1980) 775.
- [5] E.H. Roderick, R.H. Williams, *Metal Semiconductor Contacts*, Clarendon Press, Oxford, 1988, p. 201.
- [6] A. Czernik, H. Palm, W. Cabanski, M. Shultz, V. Suckow, *Appl. Phys. A* 55 (1992) 180.
- [7] A.K. Vijh, G. Belanger, R. Jacques, *Int. J. Hydrogen Energy* 15 (1990) 789.
- [8] A.K. Vijh, G. Belanger, R. Jacques, *Int. J. Hydrogen Energy* 17 (1992) 479.
- [9] A.K. Vijh, G. Belanger, R. Jacques, *J. Mater. Sci. Lett.* 12 (1993) 113.
- [10] F.-R.F. Fan, G.A. Hope, A.J. Bard, *J. Electrochem. Soc.* 129 (1982) 1647.
- [11] F.-R.F. Fan, R.G. Keil, A.J. Bard, *J. Am. Chem. Soc.* 105 (1983) 220.
- [12] H. Morisaki, H. Ono, K. Yazawa, *J. Electrochem. Soc.* 135 (1998) 381.
- [13] H. Morisaki, H. Ono, K. Yazawa, *Proc. Electrochem. Soc. (Photoelectrochem. Electrosynthesis Semiconductor Mater.)* 88 (1988) 436.
- [14] H. Morisaki, H. Ono, K. Yazawa, *J. Electrochem. Soc.* 136 (1989) 1710.
- [15] C.-A. Chang, *J. Appl. Phys.* 59 (1986) 3116.
- [16] C.A. Dimitriadis, E.K. Polychroniadis, E.K. Evangelou, G.E. Giakoumakis, *J. Appl. Phys.* 70 (1991) 3019.
- [17] S.R. Das, D.-X. Xu, J. Phillips, J. McCaffrey, L. LeBrun, A. Naem, in: S.P. Murarka, K. Rose, T. Ohmi, T. Seidel (Eds.), *Mater. Res. Soc. Symp. Proc.*, Vol. 318, Materials Research Society, Pittsburgh, PA, 1994, p. 129.
- [18] K. Maex, M. Van Rossum, A. Reader, in: K. Maex, M. Van Rossum (Eds.), *EMIS Trans Data Review Series*, 1995, p. 14.
- [19] U. Diebold, L. Zhang, J.F. Anderson, P. Mrozek, *J. Vac. Sci. Technol. A* 14 (1996) 1679.
- [20] E.P. Domashevskaya, Y.A. Yurakov, V.M. Kashkarov, *Thin Solid Films* 298 (1997) 135.
- [21] S.J. Naftel, I. Coulthard, T.K. Sham, D.-X. Xu, L. Erickson, S.R. Das, *Thin Solid Films* 58 (1997) 308.
- [22] A. Rahman, C.W. Bates, Jr., A.F. Marshall, S.B. Qadri, T. Bari, *Mater. Lett.* 39 (1999) 343.
- [23] D.M. Solina, R.W. Cheary, P.D. Swift, S. Dligatch, G.M. McCreddie, B. Gong, P. Lynch, *Thin Solid Films* 372 (2000) 94.
- [24] C. Detavernier, R. De Gryse, R.L. Van Meirhaeghe, F. Cardon, G.-P. Ru, X.-P. Qu, B.-Z. Li, R.A. Donaton, K. Maex, *J. Vac. Sci. Technol. A* 18 (2000) 470.
- [25] J. Shi, D. Kojima, M. Hashimoto, *J. Appl. Phys.* 88 (2000) 1679.
- [26] G.A. Hope, F.-R.F. Fan, A.J. Bard, *J. Electrochem. Soc.* 130 (1983) 1488.
- [27] F.F. Fan, D. Cliffel, A.J. Bard, *Anal. Chem.* 70 (1998) 2941.
- [28] Y. Zu, Z. Ding, J. Zhou, Y. Lee, A.J. Bard, *Anal. Chem.* 73 (2001) 2153.
- [29] G. Sprintschnik, H. Sprintschnik, P.P. Kirsch, D.G. Whitten, *J. Am. Chem. Soc.* 99 (1977) 4947.
- [30] A. Juris, V. Balzani, F. Barigelletti, S. Campagna, P. Belser, A. Von Zelewsky, *Coord. Chem. Rev.* 84 (1988) 85.
- [31] F. Pichet, J.H. Beck, C.M. Elliot, *J. Phys. Chem. A* 103 (1999) 6263.
- [32] C.M. Elliot, E.S. Hershenhart, *J. Am. Chem. Soc.* 104 (1982) 7519.
- [33] J.O'M. Bockris, A.K.N. Reddy, *Modern Electrochemistry*, Vol. 2, Plenum Press, New York, 1970, pp. 1153–1156, 1223–1251.
- [34] B.E. Conway, L. Bai, *J. Electroanal. Chem.* 198 (1986) 149.
- [35] E.J. Yeager, *J. Electrochem. Soc.* 128 (1981) 160C.
- [36] B.E. Conway, in: A. Wieckowski (Ed.), *Interfacial Electrochemistry: Theory, Experimental and Applications*, Marcel Dekker, New York, 1999, pp. 135–148.
- [37] R. Gomez, H.S. Yee, G.M. Bommarito, J.M. Feliu, H.D. Abruna, *Surf. Sci.* 335 (1995) 101.
- [38] C.A. Lucas, N.M. Markovic, P.N. Ross, *Phys. Rev. B* 56 (1997) 3651.
- [39] E. Herrero, S. Glazier, L.J. Buller, H.D. Abruna, *J. Electroanal. Chem.* 461 (1999) 121.
- [40] A.J. Bard, L.R. Faulkner, *Electrochemical Methods: Fundamentals and Applications*, 2nd ed., Wiley, New York, 2000, pp. 239–241.
- [41] J. Ye, J. Liu, Z. Zhang, J. Hu, S. Dong, Y. Shoa, *J. Electroanal. Chem.* 508 (2001) 123.
- [42] C. Beriet, D. Pletcher, *Electroanal. Chem.* 361 (1993) 93.
- [43] K. Winkler, *J. Electroanal. Chem.* 388 (1995) 151.
- [44] C.M. Pharr, P.R. Griffiths, *Anal. Chem.* 69 (1997) 4665.
- [45] C.M. Pharr, P.R. Griffiths, *Anal. Chem.* 69 (1997) 4673.
- [46] D.O. Wipf, A.J. Bard, *J. Electrochem. Soc.* 138 (1991) 469.
- [47] A.J. Bard, M.V. Mirkin, P.R. Unwin, D.O. Wipf, *J. Phys. Chem.* 96 (1992) 1861.
- [48] T.J. Kingzett, C.A. Ladas, *J. Electrochem. Soc.* 122 (1975) 1729.
- [49] R.J. Blattner, C.A. Evans, Jr., S.S. Lau, J.W. Mayer, B.M. Ullrich, *J. Electrochem. Soc.* 122 (1975) 1732.
- [50] X.-H. Xu, A.J. Bard, *Langmuir* 10 (1994) 2409.
- [51] X.-H. Xu, A.J. Bard, *J. Am. Chem. Soc.* 117 (1995) 2627.